Thulium-doped $Ca_4GdO(BO_3)_3$ crystals. An investigation of radiative and non-radiative processes

2000 J. Phys.: Condens. Matter 12 5495

(http://iopscience.iop.org/0953-8984/12/25/313)

J. Phys.: Condens. Matter **12** (2000) 5495–5505. Printed in the UK PII: S0953-8984(00)13025-5

Thulium-doped $Ca_4GdO(BO_3)_3$ crystals. An investigation of radiative and non-radiative processes

G Dominiak-Dzik†, W Ryba-Romanowski†, S Gołąb† and A Pajączkowska‡

† Institute of Low Temperature and Structure Research, Polish Academy of Sciences, 2 Okólna Street, 50-950 Wrocław, Poland

‡ Institute of Electronic Materials Technology, 133 Wólczyńska Street, 01-919 Warsaw, Poland

Received 3 April 2000

Abstract. An extensive investigation of optical properties was carried out for Tm^{3+}-doped $Ca_4GdO(BO_3)_3$ crystals in the 5–300 K temperature range. Based on absorption and emission spectra at 5 K, crystal field levels of active ions have been located. Non-equivalent sites for Tm^{3+} in the $Ca_4GdO(BO_3)_3$ matrix have been demonstrated. Lifetimes and the fluorescence dynamics were studied as a function of temperature and concentration of thulium ions. The Judd–Ofelt analysis of absorption spectra and the Inokuti–Hirayama model for energy transfer between activator ions provided information on radiative processes and non-radiative relaxation of excited states. Additionally, multiphonon emission was taken into account to explain a very strong quenching of the $^3H_4$ and the $^3F_4$ fluorescence.

1. Introduction

In recent years there has been a great interest in non-linear optical materials that allow production of a visible laser beam by second harmonic generation (SHG). Calcium gadolinium oxoborate $Ca_4GdO(BO_3)_3$ (GdCOB) is a new efficient non-linear optical crystal [1], belonging to the rare earth calcium borate group with general composition $Ca_4RB_3O_{10}$ (R = La–Lu, Y). Additionally, it exhibits a large transparency region and high damage threshold [1, 2]. It has been demonstrated that a neodymium-doped $Ca_4GdO(BO_3)_3$ crystal combines advantageously non-linear optical properties with an ability to amplify light and is of interest as a self-frequency doubling material [3, 4].

The Tm^{3+} ion plays an important role in solid-state laser materials. Thulium lasers are of interest as sources of light in the near infrared spectral region. The light emitted around 1.5 and 2 μm is considerably less dangerous for the human eye than light emitted by Nd^{3+}-doped materials.

The investigation of optical properties of Tm^{3+} ions in the $Ca_4GdO(BO_3)_3$ matrix can provide knowledge of the contribution of radiative and non-radiative processes in excited state relaxation.

2. Growth and brief structural description

The growth technique for the calcium rare-earth oxoborate $Ca_4REB_3O_{10}$ (RE—rare earth ions) crystals was described elsewhere [1, 5]. $Ca_4GdO(BO_3)_3$ melts congruently at 1480 °C

0953-8984/00/255495+11$30.00

so the Czochralski method was used to obtain the $Ca_4GdO(BO_3)_3$ single crystals doped with Tm^{3+} ions. The nominal concentration of Tm^{3+} ions was $x = 0.5$, 1, 6 and 12 at.%. The appropriate values of ions number per cubic centimetre are 0.22, 0.44, 2.6 and 5.2×10^{20}, respectively. The chemical formula of the crystal is $Ca_4Gd_{1-y}Tm_yO(BO_3)_3$ where $y = 0.01x$ means concentration of thulium ions.

The crystal structure of $LnCa_4O(BO_3)_3$ was resolved by Ilyukhin and Dzhurinskii [6]. $Ca_4GdO(BO_3)_3$ belongs to the calcium rare-earth oxoborate family and is isostructural to the calcium fluoroborate $Ca_5(BO_3)F$ [7], which is related to the fluoroapatite structure $Ca_5(PO_4)F$ [8]. The structure is monoclinic with the space group Cm. The Gd^{3+} ion, coordinated by six oxygen ions, is in a very distorted octahedron and has C_s symmetry. In GdCOB there are two kinds of Ca^{2+} site: Ca(1) in a slightly distorted octahedral and Ca(2) with eightfold coordination. According to structural studies [6], some disorder in the distribution of Gd and Ca ions with respect to their ideal site positions occur. In the real structure 14% of Ca ions replace Gd ions in their sites (0.86 Gd + 0.14 Ca for the unit cell), which can create point defects and non-identical local environment around Gd sites. The Tm^{3+} ion, introduced as a dopant into the $Ca_4GdO(BO_3)_3$ crystal, replaces the Gd^{3+} ion.

Crystals were grown in the ⟨010⟩ direction so the b axis was perpendicular to the ac plane. $Ca_4GdO(BO_3)_3$ is biaxial and the crystallophysical axes (X, Y, Z) are not in coincidence with the crystallographic axes (a, b, c). The divergence of these two systems is: $b \parallel Y$, $(a, Z) = 26^\circ$, $(c, X) = 15^\circ$. Samples were oriented according to crystallophysic axes—each face was cut perpendicular to one of the principal axes of the optical indicatrix. The transparency and the optical quality of crystals were good.

3. Experimental procedures

Optical absorption was recorded by using a Cary-2300 spectrophotometer that operates from 185 nm to 3.1 μm. The spectral resolution was 0.2 nm in UV–VIS and 0.8 nm in the IR region. The absorption transitions of Tm^{3+} (6 at.%) in the $Ca_4GdO(BO_3)_3$ crystal were acquired at 5 K with unpolarized light. The oriented sample was used to measure absorption line strengths at 300 K with polarized light.

Emission spectra were acquired at 5 K and room temperature. The samples were excited by a Surelite optical parametric oscillator (OPO) pumped by a third harmonic of an Nd:YAG laser. The spectra were analysed with a Zeiss model GDM 1000 grating monochromator (set to a spectral bandwidth of 2 cm^{-1}) and detected by a cooled photomultiplier. A SRS 250 boxcar integrator averaged a resulting signal. In luminescence decay time measurements an OPO was used as excitation source. Luminescent levels were excited directly. Luminescence was detected by a photomultiplier in the visible and by InSb detector in the near infrared. The resulting signal was averaged and stored using the Tektronix TDS 3052 oscilloscope. For low temperature measurements a continuous flow helium cryostat (Oxford model CF 1204) equipped with a temperature controller was used.

4. Results and discussion

4.1. Absorption data

Absorption spectra of $Ca_4GdO(BO_3)_3$ containing 6 at.% of Tm^{3+} were measured in the 2000–200 nm spectral range at 300 and 5 K and are shown in figure 1. The presented spectra consist of well resolved bands corresponding to 4f–4f electronic transitions of two lanthanide

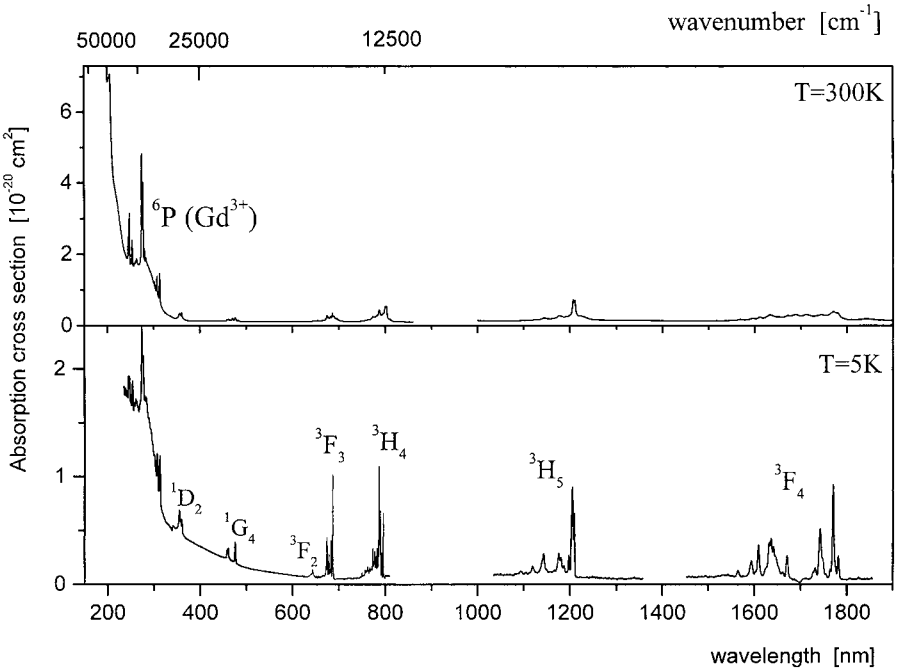

Figure 1. Absorption spectrum of Tm^{3+} ions in the $Ca_4GdO(BO_3)_3$ crystal recorded at room and 5 K temperature. Absorption bands located in the UV region (∼310 nm) are associated with Gd^{3+} transitions.

ions: Gd^{3+} and Tm^{3+}, that subsist in the crystal structure. Strong bands observed in ultraviolet range (240–320 nm) have been assigned to Gd^{3+} absorption. They are located on a broad band, which is due to point defects of the lattice. A detailed analysis of Gd^{3+} absorption and the UV absorption edge of the $Ca_4GdO(BO_3)_3$ matrix is presented in [9].

Bands observed in the 335–1850 nm spectral range correspond to transitions from the $^3H_6$ ground state to excited states of thulium. The data obtained at 5 K allowed us to analyse the $^{2S+1}L_J$ manifold structure of Tm^{3+} ions. The electronic structure of thulium ($4f^{12}$) is such that the visible and near infrared transitions involve levels having a high multiplicity ($2J + 1$) which gives a high number of Stark levels. In addition, existing disorder in the distribution of Gd and Ca ions with respect to their ideal position in the matrix leads to formation of two or more types of activator centre, each of them having a particular energy level scheme. This makes the analysis very difficult. Table 1 gives the assignment and observed energy levels of Tm^{3+} in $Ca_4GdO(BO_3)_3$. Stark level structure of the $^3H_6$ ground state has been derived from a low temperature emission corresponding to the $^1G_4 \rightarrow {}^3H_6$ transition. For all the bands studied here, the number of detected lines is greater than expected. The existence of an additional splitting within the absorption bands is exemplified in figure 2, which shows the structure of lines associated with the $^3H_6 \rightarrow {}^3F_4$ transition. Any J level of the Tm^{3+} ion in the $Ca_4GdO(BO_3)_3$ host will split into $(2J + 1)$ components, hence, for the $^3F_4$ multiplet we expect nine components. The absorption spectrum consists of nine groups of lines, each of them having a rich structure. It is clear that the absorption spectra of Tm^{3+} are too complex to provide unambiguous information on the lattice location impurities and other techniques are needed.

Table 1. Observed energy levels and overall splitting of Tm^{3+} in the $Ca_4GdO(BO_3)_3$ crystal.

$^{(2S+1)}L_J$	Energy [cm^{-1}]	ΔE [cm^{-1}]
$^3H_6$	0, 78, 170, 199, 236, 252, 282, 372, 393, 460, 500, 655, 828	828
$^3F_4$	5613, 5650, 5669, 5699, 5722, 5743, 5776, 5794, 5988, 6020, 6054, 6078, 6095, 6114, 6130, 6155, 6217, 6240, 6274, 6288	675
$^5H_5$	8268, 8292, 8306, 8322, 8347, 8420, 8463, 8473, 8510, 8563, 8749, 8775, 8938	670
$^3H_4$	12 571, 12 585, 12 624, 12 636, 12 672, 12 718, 12 749, 12 774, 12 813, 12 864, 12 888, 12 926	355
$^3F_3$	14 547, 14 568, 14 589, 14 602, 14 635, 14 667, 14 691, 14 734, 14 763, 14 833, 14 880	333
$^3F_2$	15 222, 15 258, 15 330, 15 442, 15 478, 15 515, 15 558	336
$^1G_4$	20 930, 20 957, 20 982, 21 014, 21 042, 21 554, 21 649, 21 689, 21 749, 21 775, 21 812	882
$^1D_2$	27 687, 27 728, 27 880, 27 903, 28 065, 28 167, 28 270	583

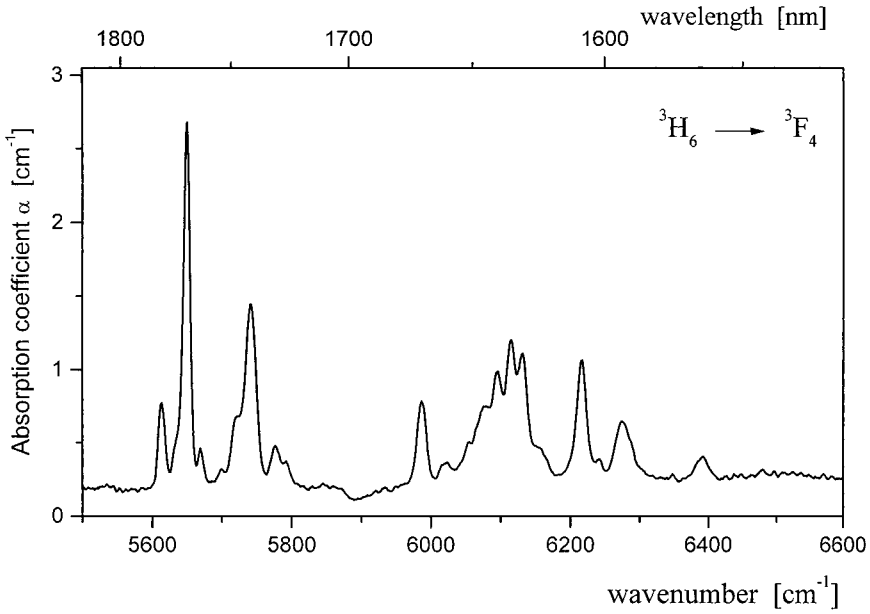

Figure 2. Absorption spectrum corresponding to the $^3H_6 \rightarrow {}^3F_4$ transition of Tm^{3+}: $Ca_4GdO(BO_3)_3$ acquired at 5 K.

4.2. The Judd–Ofelt analysis

The Judd–Ofelt model was used to predict such spectroscopic parameters as radiative transition probabilities (A_r), radiative lifetimes (τ_r) of excited states, and branching ratios (β). It is worth noting that this model refers to isotropic host materials, therefore some extension should be made with respect to anisotropic (uniaxial, biaxial) crystals. The GdCOB:Tm crystal is biaxial, so a cubic sample was cut with each face oriented perpendicular to one of the X, Y or Z crystallophysical axes. Room temperature absorption spectra were collected from the sample with 1.0 at.% (4.3×10^{19} ions cm^{-3}) of Tm^{3+}. Concentration was kept low to minimize concentration-dependent interactions between active ions. To obtain a reasonable approximation of experimental oscillator strengths, three different spectra were acquired with the electric field E of incident light parallel to the X, Y or Z axis, respectively. Absorption spectra show strong polarization dependence. Figure 3 is an example of the polarization

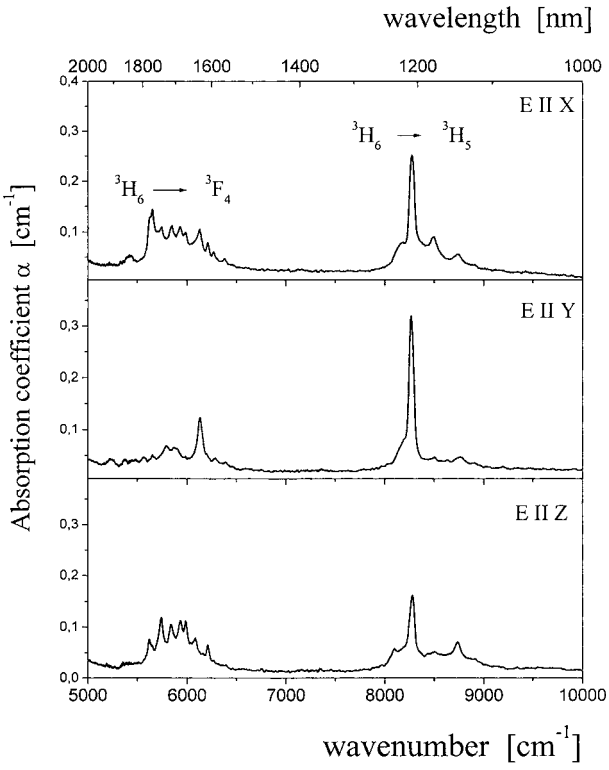

Figure 3. Room temperature polarized absorption spectra of $Ca_4GdO(BO_3)_3$: 1% Tm^{3+} recorded in the near infrared spectral range.

effect on the $^3H_6 \rightarrow {}^3F_4$ and $^3H_6 \rightarrow {}^3H_5$ transitions in the infrared regions. All transitions were assumed to be electric dipole in nature, except for the $^3H_6 \rightarrow {}^3H_5$ transition, which contains a substantial magnetic dipole moment. This magnetic dipole contribution was evaluated according to the procedure given in [10]. The $^3H_6 \rightarrow {}^1D_2$ transition was not included in our calculation due to an overlapping point defect band. Oscillator strengths $P_{X,Y,Z}$ were determined by numerical integration of five absorption bands. Next, for each transition a mean value of the oscillator strength $P_{ave} = \frac{1}{3}\sum_{i=X,Y,Z} P_i$ has been calculated and the phenomenological Ω_t parameters have been obtained by the least-squares fit between experimental and theoretical oscillator strengths. Measured and calculated data are collected in table 2. The resulting Ω_t parameters, compared to those of the other hosts, are given in table 3. The Ω_2 parameter is greater than those found in the case of Tm^{3+}-doped YAG [13] and $SrGdGa_3O_7$ [11], and comparable to that obtained for the $Tm:Y_2SiO_5$ [12] system. A low value of Ω_4 can be related to Ω_4 calculated for Tm^{3+} in the $LiNbO_3$ crystal [14]. Generally, Ω_6 parameter does not stand out from values found in the Tm^{3+}-doped crystals mentioned here.

Knowing Ω_t parameters one can calculate the radiative transition rates A_r for excited levels according to the formula:

$$A_r = \frac{64\pi^4 e^2}{3h(2J+1)\lambda^3}\frac{n(n^2+2)^2}{9}\sum_{i=2,4,6}\Omega_t|\langle f^N[L,S]J\|U^{(t)}\|f^N[L,S']J'\rangle|^2 \quad (1)$$

where n is the refractive index of the medium. For GdCOB, the evaluation of the refractive index dispersion as a function of incident wavelength is presented in [1, 3]. Calculated values

Table 2. Experimental $P_{X,Y,Z}$, average P_{ave} and calculated P_{cal} oscillator strengths for Tm^{3+} in the $Ca_4GdO(BO_3)_3$ crystal. All transitions are from the $^3H_6$ ground level to levels indicated.

Excited level	Average wavelength [nm]	Oscillator strength $P_{exp} \times 10^{-6}$					Residuals $(P_{cal} - P_{exp})$ $\times 10^{-6}$
		P_X	P_Y	P_Z	P_{ave}	P_{cal}	
$^3F_4$	1689	1.34	0.56	1.16	1.02	1.03	0.01
$^3H_5$	1183	1.32	1.07	1.06	0.87[a]	0.73	0.14
$^3H_4$	780	1.67	0.95	1.32	1.31	1.39	0.08
$^3F_3$, $^3F_2$	686	1.20	0.60	1.12	0.97	1.11	0.14
$^1G_4$	470	0.61	0.33	0.37	0.43	0.39	0.04

[a] A magnetic dipole contribution was calculated according to [10] and subtracted from the averaged experimental value.

Table 3. Values of the phenomenological parameters Ω_t [10^{-20} cm^2] for Tm^{3+} in $Ca_4GdO(BO_3)_3$ compared to those of $SrGdGa_3O_7$, Y_2SiO_5, YAG and $LiNbO_3$.

	GdCOB	$SrGdGa_3O_7$ [11]	Y_2SiO_5 [12]	YAG [13]	$LiNbO_3$ [14]
Ω_2	1.92	1.29	2.43	0.7	4.9
Ω_4	0.15	1.08	1.74	1.2	0.48
Ω_6	0.63	0.47	0.66	0.5	0.31

of the radiative transition rates for excited states of Tm^{3+} ions in the GdCOB crystal are reported in table 4. From these values it is possible to calculate the radiative lifetime of an excited state i according to the formula:

$$\frac{1}{\tau_r} = \sum_j A_r(i, j) \tag{2}$$

and the branching ratio defined as:

$$\beta = \frac{A_r(i, j)}{\sum_j A_r(i, j)} = \tau_r A_r(i, j) \tag{3}$$

where the summation is over electric and magnetic dipole transitions to all terminal j states. The values of radiative lifetimes and branching ratios are listed in table 4 too.

4.3. Emission and fluorescence lifetime data

Emission spectra of the sample doped with 0.5 at.% of Tm^{3+} ions were recorded in the 11 800–22 500 cm^{-1} (850–450 nm) spectral range after selective excitation into the $^1D_2$ and the $^1G_4$ levels. In figure 4 we present emission of Tm^{3+} ions, recorded at 5 K under excitation into the $^1G_4$ state ($\lambda_{exc} = 466$ nm) and the $^1D_2 \rightarrow {}^3F_4$ fluorescence obtained when excitation wavelength was $\lambda_{exc} = 355$ nm (see inset). We have observed strong, well resolved lines associated with the $^1G_4 \rightarrow {}^3F_4$ transition and two considerably weaker bands corresponding to the $^1G_4 \rightarrow {}^3H_6$ and to the $^1G_4 \rightarrow {}^3H_5$ emissions. Excitation into the $^1D_2$ level provides three fluorescence bands. A strong and well resolved band in the 21 200–22 250 cm^{-1} range was assigned to the $^1D_2 \rightarrow {}^3F_4$ transition, whereas a group of weak and poorly resolved lines at 27 000 cm^{-1} was identified as emission from the $^1D_2$ level to the $^3H_6$ ground state of Tm^{3+} ions. Emission lines located at 20 800 cm^{-1} were interpreted as the $^1G_4 \rightarrow {}^3H_6$ fluorescence. All those luminescence measurements provide an exceptionally rich set of data, especially with respect to the $^3F_4$ excited state and the $^3H_6$ ground state. It was very helpfully to crystal

Table 4. Calculated radiative transition rates A_r, luminescence branching ratios β and corresponding radiative lifetimes τ_{rad} and luminescence lifetimes τ_{exp} for Tm^{3+} (0.5 at.%) in $Ga_4GdO(BO_3)_3$.

Transition	Wavelength [nm]	A_r [s^{-1}]	β	τ_{rad} [μs]	τ_{exp} [μs]
$^1D_2 \rightarrow {}^3H_6$	358	1565	0.141	89.9	16.3
$^3F_4$	455	8008	0.720		
$^3H_5$	516	60	0.005		
$^3H_4$	662	893	0.080		
$^3F_3, {}^3F_2$	750	516	0.046		
$^1G_4$	1515	75	0.007		
$^1G_4 \rightarrow {}^3H_6$	469	500	0.440	880	240
$^3F_4$	650	69	0.060		
$^3H_5$	778	401	0.353		
$^3H_4$	1178	133	0.117		
$^3F_3, {}^3F_2$	1488	34	0.030		
$^3H_4 \rightarrow {}^3H_6$	781	651	0.926	1424	—
$^3F_4$	1454	49	0.069		
$^3F_5$	2299	3	0.005		
$^3F_4 \rightarrow {}^3H_6$	1689	102	1.000	9767	—

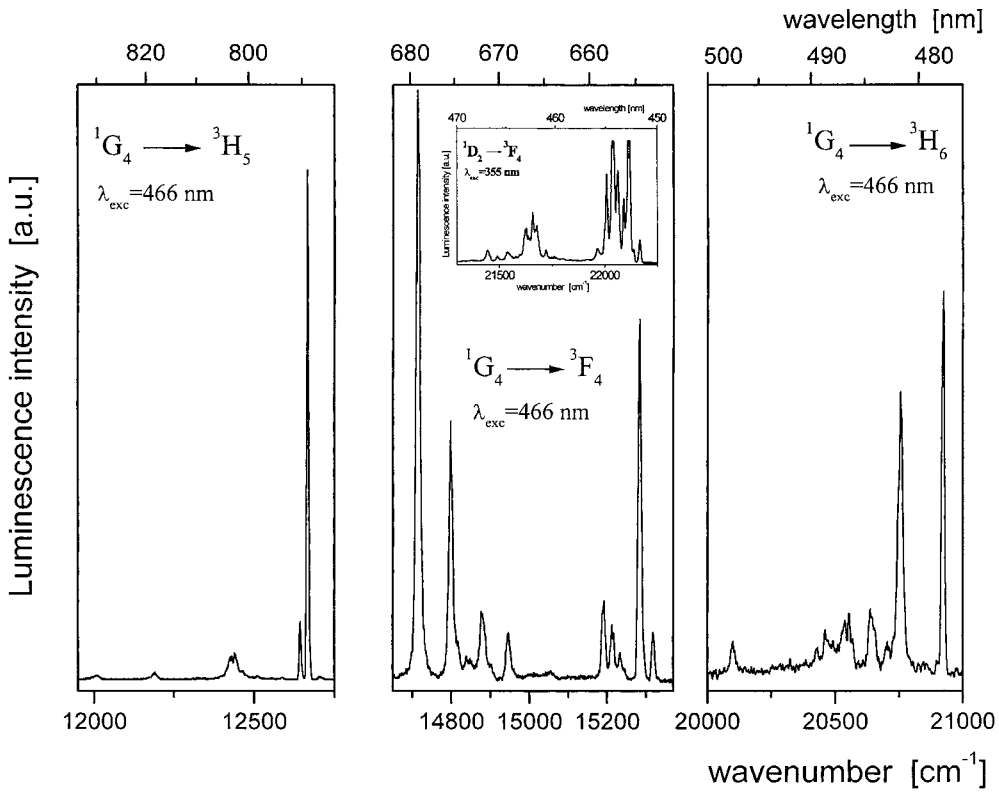

Figure 4. Luminescence spectra of Tm^{3+} in $Ca_4GdO(BO_3)_3$ under excitation into the $^1G_4$ multiplet ($\lambda_{exc} = 466$ nm) and the $^1D_2 \rightarrow {}^3F_4$ fluorescence recorded under $\lambda_{exc} = 355$ nm (inset). $T = 5$ K.

field level identification because all of the emission bands show a multi-site structure similar to that observed in absorption.

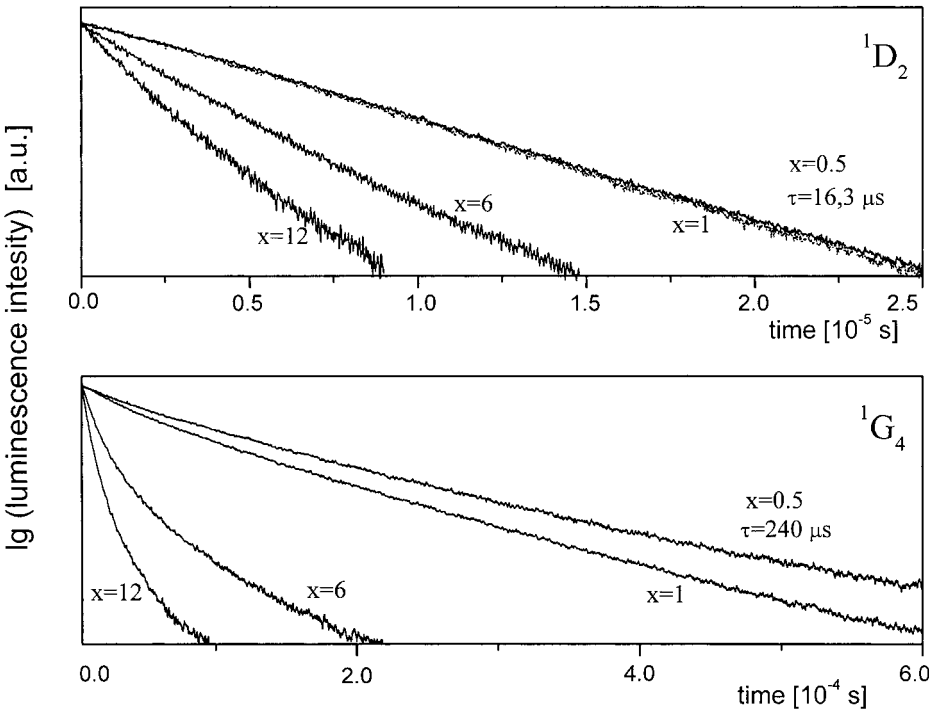

Figure 5. Room temperature $^1D_2$ (upper) and $^1G_4$ (lower) fluorescence decays in $Ca_4GdO(BO_3)_3$:x% Tm (x = 0.5, 1, 6 and 12 at.%) after pulsed excitation at 355 and 466 nm, respectively.

Luminescence originating in the $^3H_4$ and the $^3F_4$ excited states was too weak to be observed. It was a rather unexpected result: according to the Judd–Ofelt analysis radiative lifetimes τ_r for the $^3H_4$ and the $^3F_4$ levels are 1424 and 9767 μs respectively, and luminescence branching ratios β give values 0.93 for the $^3H_4 \rightarrow {}^3H_6$ transition and 1.0 for the $^3F_4 \rightarrow {}^3H_6$ transition. The lack of these emissions in experiment clearly indicates strong non-radiative processes acting in the Tm:$Ca_4GdO(BO_3)_3$ system.

The lifetime measurements of the emitting levels have been carried out under excitation with 355 nm ($^1D_2$ multiplet) and 466 nm ($^1G_4$ state). The $^1G_4$ lifetime, measured for the most dilute sample was found to be temperature independent in the 5–300 K range. Table 4 gives the experimental values of lifetimes acquired from a sample with 0.5 at.% of Tm^{3+} at room temperature. It can be seen that all luminescence lifetimes are lower than those calculated.

To obtain a more detailed insight into excited state relaxation, decay curves of luminescence were recorded for different thulium concentration, at 300 K. The effect of Tm^{3+} content on the $^1D_2$ and the $^1G_4$ lifetimes is exemplified in figure 5. Time constants, recorded for studied samples, are inset in the figure. Decays become non-exponential and faster when Tm^{3+} concentration increases. The presented decay curves give evidence that both the $^1D_2$ and the $^1G_4$ excitation is lost by a non-radiative ion–ion interaction.

4.4. Non-radiative relaxation of excited states of Tm^{3+} ions

The presence of luminescence from the $^1G_4$ level when the $^1D_2$ state is excited, a significant difference between calculated and measured lifetimes and a strong concentration dependence of

luminescence intensity clearly indicate the contribution of non-radiative processes to relaxation of the excited state of Tm^{3+} in the $Ca_4GdO(BO_3)_3$ crystal. Therefore, multiphonon and activator–activator interactions should be considered in detail.

4.4.1. Multiphonon emission of Tm^{3+} in GdCOB. When we assume a weak excitation and the absence of non-radiative energy transfer, an ion in excited state decays with a measured lifetime τ_{exp} given by

$$\frac{1}{\tau_{exp}} = A_{rad} + A_{ph} \tag{4}$$

where A_{rad} is the radiative transition rate and A_{ph} is non-radiative transition rate due to multiphonon emission. Radiative transitions and relaxation by emission of phonons govern the decay when the concentration of active ions is sufficiently low. Usually, phonons with the highest energy are considered since they easily conserve the energy gap between two states bridged by multiphonon relaxation. In the $Tm:Ca_4GdO(BO_3)_3$ system, the largest phonon frequency ($\hbar\omega_{ph} = 1260\ cm^{-1}$) is associated with the stretching vibrations of the $(BO_3)^{3-}$ anion group.

The energy gap between the $^3H_4$ and the $^3H_5$ levels is about 3400 cm^{-1}, therefore the number of phonons needed to cover the energy gap is only three. The $^3F_4$ and the $^3H_6$ levels are separated by 4800 cm^{-1}. This energy separation is very close to that observed between the $^4F_{3/2}$ and $^4I_{15/2}$ states ($\Delta E \sim 4900\ cm^{-1}$) in the $Nd:Ca_4GdO(BO_3)_3$ system [15]. For the $^4F_{3/2}$ level of the Nd^{3+} ion the multiphonon emission rate A_{ph} was found to be $\sim$9000 s^{-1} at 300 K and the $^3F_4$ quantum efficiency, defined as $\eta = \tau_{exp}/\tau_{rad}$, was about 15%. If we assume 9000 s^{-1} as a probable multiphonon emission rate A_{ph} for the $^3F_4$ thulium level, we obtain the quantum efficiency of the $^3F_4$ fluorescence of about 1% at best. It seems that ion–lattice coupling is much stronger in Tm^{3+}-doped GdCOB than in the $Nd:Ca_4GdO(BO_3)_3$ system. This can explain the lack of the $^3F_4$ and the $^3H_4$ fluorescence in our observations.

The presence of luminescence from the $^1G_4$ level when the $^1D_2$ state is excited shows that the $^1G_4$ state is populated non-radiatively by cross-relaxation or/and by multiphonon emission. The time dependence of the $^1D_2$ population, reported in figure 5, exhibits a strong decrease when Tm^{3+} concentration increases. The time constant of 6.7 μs was determined from the long-time part of the decay for the sample with 12 at.% of thulium. The shortening of the $^1D_2$ lifetime (from 16.3 to 6.7 μs) indicates that cross-relaxation takes place and quenches the $^1D_2$ luminescence. The cross-relaxation quenching rate A_{CR} was calculated by

$$A_{CR} = 1/\tau - 1/\tau_0 \tag{5}$$

where τ_0 and τ are lifetimes of the 0.5 and 12 at.% doped sample, respectively. A value of the order of 10^5 s^{-1} was obtained, which is similar to that obtained for the $^3H_4 \rightarrow {}^3H_6$ fluorescence of 7 mol% TmF_3:BIZYT [16]. The cross-relaxation quantum efficiency of about 60% was estimated according to relation $\eta = 1 - \tau/\tau_0$. It seems that in spite of a significant energy gap ($\Delta E \sim 6000\ cm^{-1}$) multiphonon emission is active, too.

The energy separation between the $^1G_4$ and the $^3F_2$ levels is of the order of 5300 cm^{-1}, therefore four phonons with the highest energy are needed to cover this energy gap. The multiphonon emission rate, calculated by subtracting the radiative contribution from the fluorescence lifetime, was found to be 3060 s^{-1}.

4.4.2. Non-radiative energy transfer. The time dependences of the $^1D_2$ and the $^1G_4$ populations when levels are directly excited were studied by considering the decays of the fluorescence at 22 000 cm^{-1} ($^1D_2 \rightarrow {}^3F_4$) and 15 300 cm^{-1} ($^1G_4 \rightarrow {}^3F_4$) for samples with

0.5, 1, 6 and 12 at.% of Tm^{3+} ions. Thulium ions play the role of donors and acceptors simultaneously. Tm^{3+} fluorescence acquired from the sample with 0.5 at.% of Tm^{3+} decays exponentially in both considered emissions. When the content of activator increases, decays deviate from simple exponential dependence and for samples with 6 and 12 at.% of Tm^{3+} observed decays become faster and strongly non-exponential owing to the self-quenching of Tm^{3+} fluorescence. This process occurs via cross-relaxation and is frequently observed in crystals containing high concentration of active ions [12, 17, 18].

The initial non-exponential portion of the decay is attributed to relaxation by direct Tm^{3+}–Tm^{3+} energy transfer. When the concentration is low (1 at.%) the acceptor concentration is low too, and only a small fraction of the total number of excited donors are within the effective interaction sphere of an acceptor. Therefore, direct donor–acceptor relaxation contributes less to the overall decay and the non-exponential portion of the decays in figure 5 is correspondingly smaller.

The decay curves can be fitted by the Inokuti–Hirayama model [19], which is adequate in describing energy transfer processes where donor–acceptor transfer is much faster than migration. Assuming dipole–dipole interactions between the ions, the time evolution of the donor emission intensity is:

$$\Phi(t) = A \exp[-(t/\tau_0) - \alpha(t/\tau_0)^{3/s}] \tag{6}$$

where A is a constant, $\Phi(t)$ is emission intensity after pulse excitation, $s = 6$ for dipole–dipole interactions between the ions, τ_0^{-1} is the intrinsic decay probability of the donor ions involved in the energy transfer process in the absence of acceptors and α is the parameter described as:

$$\alpha = 4/3\pi\Gamma(1 - 3/s)N_a R_0^3. \tag{7}$$

In this equation $s = 6$, thus $\Gamma(1 - 3/s) = \Gamma(1/2) = 1.77$ where Γ is the Euler function, N_a is the concentration of acceptor ions and R_0 is the critical transfer distance defined as that separation at which the probability of energy transfer between a donor–acceptor pair is equal to the intrinsic decay rate τ_0^{-1}. When the energy transfer process is a cross-relaxation within the system of identical activators, the acceptor concentration is identical to that of activator [20]. Fitting of the $^1G_4$ fluorescence decay curve to equation (6) gives the value $\alpha = 1.92$ for the 6 at.% doped crystal. The N_a concentration was calculated as 2.6×10^{20} ions cm^{-3}. From equation (6) we have determined the critical transfer distance R_0 as 9.99 Å, which is similar to that obtained for YSO:Tm^{3+} [12]. This value and lifetime $\tau_0 = 240$ μs were used to calculate the donor–acceptor interaction parameters given by the $C_{da} = R_0^6\tau_0^{-1}$ relation. The C_{da} value was found to be 4.1×10^{-51} m^6 s^{-1}. This value is of the same order of magnitude as those obtained for Tm^{3+} (the $^3H_4$ level) doped $SrGdGa_3O_7$ [11], YAG [17] and YVO_4 [21], for which the C_{da} parameter was determined as 2.2, 2.7 and 1.8×10^{-51} m^6 s^{-1}, respectively. The energy transfer probability $W_{da} = C_{da}R_0^{-6}$ was estimated as 4160 s^{-1} for the self-quenching emission of Tm^{3+} in the $Ca_4GdO(BO_3)_3$ matrix.

With time t, the number of donors having unexcited acceptors within the critical transfer radius diminishes and intrinsic decay rate is more competitive with energy transfer. Thus, the final portions of the decays in figure 5 become exponential.

For the 12 at.% Tm^{3+}-doped crystal, the α value differs insignificantly from the value obtained for lower thulium content. This indicates that additional processes like energy migration among the donor system are competitive and influence direct donor–acceptor energy transfer, so the Inokuti–Hirayama model is no longer applicable. This phenomenon is typical of so-called 'static' and diffusion limited energy transfer interactions and is observed for other systems [12, 18].

5. Conclusion

The optical properties of thulium-doped $Ca_4GdO(BO_3)_3$ crystals have been investigated in more detail. Absorption and emission spectra have been recorded at low temperature to obtain the best description of the crystal-field levels. Room temperature, polarized absorption spectra have been analysed within the Judd–Ofelt framework to have information on radiative processes and excited state radiative lifetimes. No fluorescence from the $^3F_4$ and the $^3H_4$ states was observed. Processes contributing to the relaxation of excited states of Tm^{3+} ions have been considered. The $^1G_4$ and the $^1D_2$ fluorescence decay curves as functions of thulium concentration have been studied. The results showed that multi-phonon relaxation and activator–activator interaction play a dominant role in the relaxation of thulium excited states. For a self-quenching of Tm^{3+} emission, a critical distance $R_0 = 9.99$ Å and the interaction parameter $C_{da} = 4.1 \times 10^{-51}$ ($m^6\ s^{-1}$) have been obtained by the Inokuti–Hirayama model.

Acknowledgment

The Committee for Scientific Research supported this work under grant No 8T 11B 007 16.

References

[1] Aka G, Kahn-Harari A, Vivien D, Benitez J M, Salin F and Godard J 1996 *Eur. J. Solid State Inorg. Chem.* **33** 727
[2] Furuya H, Yoshimura M, Kobayashi T, Murase K, Mori Y and Sasaki T 1999 *J. Cryst. Growth* **198/199** 560
[3] Vivien D, Mougel F, Aka G, Kahn-Harari A and Pelenc D 1998 *Laser Phys.* **8** 759
[4] Mougel F, Dardenne K, Aka G, Kahn-Harari A and Vivien D 1999 *J. Opt. Soc. Am.* B **16** 164
[5] Aka G, Bloch L, Godard J, Kahn-Harari A, Vivien D and Salin F, CRISMATEC Company 1995 Cristaux non linéaires et leur applications *French Patent* FR 95/01963
[6] Ilyukhin A B and Dzhurinskii F B 1993 *Russ. J. Inorg. Chem.* **36** 847
[7] Lei S, Qingzhen H, Yifan Z, Aidong J and Chuangtian C 1989 *Acta Crystallogr.* C **45** 1861
[8] Fletcher J G, Glasse F P and Howie A 1991 *Acta Crystallogr.* C **47** 12
[9] Dominiak-Dzik G, Ryba-Romanowski W, Gołąb S, Macalik L, Hanuza J and Pajączkowska A *J. Mol. Struct.* at press
[10] Carnall W T, Fields P R and Rajnak K 1968 *J. Chem. Phys.* **49** 4412
[11] Ryba-Romanowski W, Gołąb S, Sokólska I, Dominiak-Dzik G, Zawadzka J, Berkowski M, Fink-Finowicki J and Baba M 1999 *Appl. Phys.* B **68** 199
[12] Li C, Lagriffoul A, Moncorge R, Souriau J C, Borel C and Wyon Ch 1994 *J. Lumin.* **62** 157
[13] Weber M J, Varitimos T E and Matsinger B H 1973 *Phys. Rev.* B **8** 47
[14] Núñez L, Tocho J O, Sanz-Garcia J A, Rodriguez E, Cussó F, Hanna D C, Tropper A C and Large A C 1993 *J. Lumin.* **55** 253
[15] Mougel F, Aka G, Kahn-Harari A, Hubert H, Benitez J M and Vivien D 1997 *Opt. Mater.* **8** 161
[16] Brenier A, Pedrini C, Moine B, Adam J L and Pledel C 1990 *Phys. Rev.* B **41** 5364
[17] Armagan G, Buoncristiani A M and DiBartolo B 1992 *Opt. Mater.* **1** 11
[18] Ryba-Romanowski W, Berkowski M, Viana B and Aschehoug P 1997 *Appl. Phys.* B **64** 525
[19] Inokuti M and Hirayama F 1965 *J. Chem. Phys.* **43** 1978
[20] Lupei V 1991 *J. Lumin.* **48/49** 157
[21] Bettinelli M, Ermeneux F S, Moncorge R and Cavalli E 1998 *J. Phys.: Condens. Matter* **10** 8207